Technical University of Denmark

DTU

The future sea-level rise contribution of Greenland's glaciers and ice caps

Machguth, H.; Rastner, P.; Bolch, T.; Mölg, N.; Sørensen, Louise Sandberg; Aðalgeirsdottir, G.; van Angelen, J. H.; van den Broeke, M. R.; Fettweis, X.

Link back to DTU Orbit

DTU Library
Technical Information Center of Denmark

The future sea-level rise contribution of Greenland's glaciers and ice caps

H Machguth[1,2]**, P Rastner**[1]**, T Bolch**[1,3]**, N Mölg**[1]**, L Sandberg Sørensen**[4]**,
G Aðalgeirsdottir**[5]**, J H van Angelen**[6]**, M R van den Broeke**[6] **and
X Fettweis**[7]

[1] Department of Geography, University of Zurich, Switzerland
[2] Geological Survey of Denmark and Greenland (GEUS), Copenhagen, Denmark
[3] Institute for Cartography, Technical University Dresden, Germany
[4] Technical University of Denmark, Kongens Lyngby, Denmark
[5] Danish Meteorological Institute (DMI), Copenhagen, Denmark
[6] Institute for Marine and Atmospheric Research (IMAU), Utrecht, The Netherlands
[7] Department of Geography, University of Liège, Liège, Belgium

E-mail: horst.machguth@geo.uzh.ch

Abstract

We calculate the future sea-level rise contribution from the surface mass balance of all of Greenland's glaciers and ice caps (GICs, $\sim$90 000 km^2) using a simplified energy balance model which is driven by three future climate scenarios from the regional climate models HIRHAM5, RACMO2 and MAR. Glacier extent and surface elevation are modified during the mass balance model runs according to a glacier retreat parameterization. Mass balance and glacier surface change are both calculated on a 250 m resolution digital elevation model yielding a high level of detail and ensuring that important feedback mechanisms are considered. The mass loss of all GICs by 2098 is calculated to be 2016 $\pm$ 129 Gt (HIRHAM5 forcing), 2584 $\pm$ 109 Gt (RACMO2) and 3907 $\pm$ 108 Gt (MAR). This corresponds to a total contribution to sea-level rise of 5.8 $\pm$ 0.4, 7.4 $\pm$ 0.3 and 11.2 $\pm$ 0.3 mm, respectively. Sensitivity experiments suggest that mass loss could be higher by 20–30% if a strong lowering of the surface albedo were to take place in the future. It is shown that the sea-level rise contribution from the north-easterly regions of Greenland is reduced by increasing precipitation while mass loss in the southern half of Greenland is dominated by steadily decreasing summer mass balances. In addition we observe glaciers in the north-eastern part of Greenland changing their characteristics towards greater activity and mass turnover.

Keywords: Greenland, glaciers and ice caps, sea level rise contribution, climate model output, glacier retreat parameterization

1. Introduction

Glaciers and ice caps (GICs) of most regions in the world are currently undergoing strong changes. Retreat and mass loss are also observed on the GICs of Greenland (e.g. Knudsen and Hasholt 2008, Bolch *et al* 2013). The recently published glacier inventory of Greenland (Rastner *et al* 2012) revealed that the surface area of GICs amounts to $\sim$90 000 km^2 ($\sim$12% of the total GICs on earth), considerably more than previously estimated. Hence there is a considerable potential for sea-level rise that has so far received limited attention compared to other Arctic regions such as Svalbard (e.g. Nuth *et al* 2010) or the Canadian Arctic (e.g. Gardner *et al* 2011).

In the majority of studies focusing on future changes of GICs, these are treated as abstracted and simplified

objects. For instance Raper and Braithwaite (2006) address GICs as size distributions of glacier areas and volumes in 1° latitude/longitude cells. Radić and Hock (2011) approximate the hypsometry of mountain glaciers by linearly increasing the area per elevation-band from zero at the terminus to a maximum at the mean altitude and a linear decrease above. Such abstractions of glaciers allow for a computationally efficient handling of very large glacier samples. However, it is difficult to assess to what degree abstract representations of glaciers are representative for real conditions.

These issues motivate the development of modeling approaches aiming at a more realistic representation of large glacier samples including important mechanisms such as the feedback of glacier thinning on glacier mass balance. The impact of this feedback process strongly depends on the hypsometry of each individual glacier: flat glaciers can loose considerable portion of their accumulation area due to surface lowering while steep glaciers are less sensitive to this effect (Jiskoot *et al* 2009).

The above considerations point out the importance of taking characteristics of individual glaciers into account when modeling future extent and volume changes. On GICs a high level of detail is required for accurate representation of complex glacier topography and surface mass balance distribution. Sufficient input data for comprehensive modeling of ice dynamics and mass balance is only available for a few well studied (and mostly small) glaciers (e.g. Zwinger and Moore 2009). For larger glacier samples more simple approaches are applied: Huss *et al* (2008, 2010a), Salzmann *et al* (2012) combined glacier mass balance models with the so called 'Δh glacier retreat parameterization' (Huss *et al* 2010b) to model future glacier extent and volume of glacierized catchments in the Swiss Alps.

In the present study we apply a similar approach as in Salzmann *et al* (2012) to calculate future scenarios of Greenland's GICs from the year 2000 to 2098 and their contribution to sea-level rise. We combine DEMs, satellite derived glacier inventory data, surface elevation changes measured from ICEsat, mass balance and ice thickness measurements as well as gridded climate model output to achieve a more realistic representation of Greenland's GICs in future-scenario calculations. Glacier surface mass balance and glacier retreat scenarios are computed for six selected regions and ultimately upscaled to all of Greenland's GICs.

2. Study area and data

The newly established Greenland glacier inventory (Rastner *et al* 2012) was used as baseline information of glacier extents. The inventory includes all GICs on Greenland at a spatial resolution of 30 m and is derived from Landsat scenes acquired mostly in between 1999 and 2002. GICs are divided into three classes of connectivity to the ice sheet: CL0 (no connection), CL1 (weakly connected) and CL2 (strongly connected). CL0 and CL1 are glaciers dynamically independent of the ice sheet, CL2 ice bodies are of local character but dynamically not independent from the ice
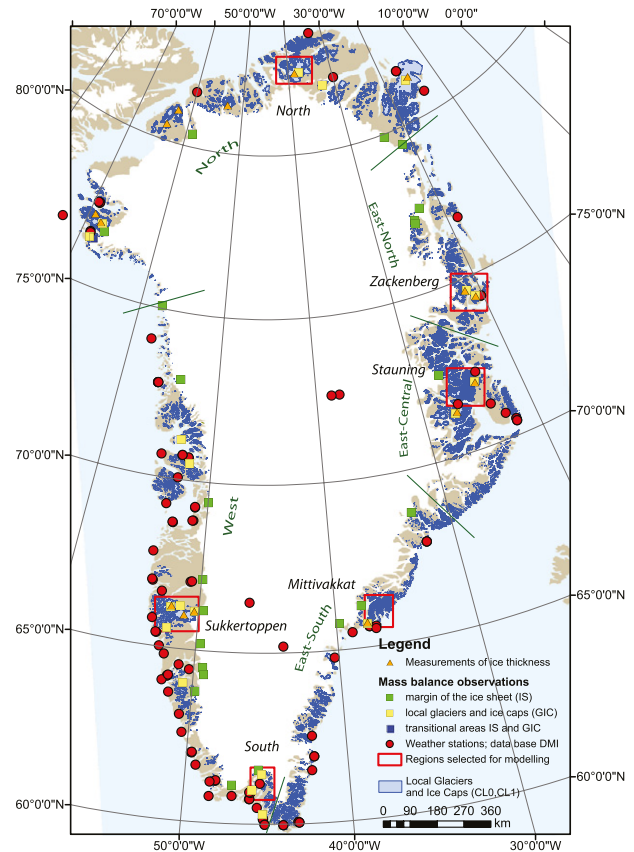
Figure 1. The six selected regions (red rectangles) and locations of field observations are marked on the map. The five sectors used for the extrapolation of the modeled mass loss are shown in dark-green.

sheet. According to Rastner *et al* (2012), the area of Greenland's GICs amounts to ~90 000 km² (CL0 and CL1) or ~130 000 km² (all three connectivity classes). The area of CL0 and CL1 glaciers amounts to ~150% of earlier estimates (e.g. Weidick and Morris 1998, Radić and Hock 2011).

Six regions of Greenland were selected for detailed modeling of glacier mass balance and glacier retreat (table 1 and figure 1). The regions were chosen to represent the different climatic regions of Greenland and to achieve an optimum availability of input and validation data for the modeling. All of the six regions include glaciers with mass balance observations, ice thickness measurements and meteorological stations of the Danish Meteorological Institut (DMI): (1) the southernmost tip of Greenland (henceforward called 'South'), (2) the Sukkertoppen area in the south-west dominated by two larger ice caps ('Sukkertoppen'), (3) a region in the south-east including Mittivakkat glacier, Greenland's only GIC with a longer-term mass balance series ('Mittivakkat'), (4) the Stauning Alper in the central east comprising rugged mountain terrain with valley glaciers but also ice caps ('Stauning'), (5) the area around the Zackenberg research station in the north-east ('Zackenberg') and (6) in the far north the area around Hans Tausen ice cap ('North'). In total these six regions include 17 660 km² of GICs, corresponding to 20% of all CL0 and CL1 glaciers in Greenland.

Table 1. Overview of the six selected regions and the central region specific model calibration parameters. P_{corr} values vary depending on whether $\sum B_a$ *minimum*, *maximum* or *intermediate* is used in calibration. For simplicity only values of P_{corr} for the *intermediate* calibration are given. A dash ('—') indicates that no correction was applied.

	North	Zackenberg	Stauning	Mittivakkat	South	Sukkertoppen
h_{max} (m)	400	350	500	800	—	500
C_0 (W m^{-2})	−45	−45	−45	−45	−45	−45
C_1 (W m^{-2} °C^{-1})	12	12	12	14	14	12
α_i	0.4	0.4	0.4	0.35	0.35	0.4
$\sum B_a$ *maximum* (m w.e.)	−1.3	−4.4	−2.9	−10	−5.1	−3.6
$\sum B_a$ *intermediate* (m w.e.)	−1.8	−6.1	−4.1	−14	−7.9	−5
$\sum B_a$ *minimum* (m w.e.)	−2.3	−7.8	−5.3	−18	−10.7	−6.4
Bias correction T	Yes	Yes	No	Yes	Yes	Yes
RACMO2 mean P_{corr}	1.06	1.01	1.02	0.83	0.84	1.18
HIRHAM5 mean P_{corr}	0.93	0.89	1.12	1.13	0.84	0.88
MAR mean P_{corr}	0.94	1.14	0.82	1.49	0.79	0.88
RACMO2 T_{offset} (K)	—	—	−0.5	0.75	—	−1.0
HIRHAM5 T_{offset} (K)	—	—	−0.5	−1.5	0.5	—
MAR T_{offset} (K)	—	—	1.5	−1.5	1.5	—

For all regions we used the 90 m resolution DEM (down-sampled to 250 m resolution) of the Greenland Ice Mapping Project (Howat *et al* 2013), currently one of the best DEM available for Greenland (Rastner *et al* 2012). The mass balance model is driven from gridded climate model output and we use regional climate model (RCM) data from three different sources: (1) a ∼25 km resolution run of HIRHAM5 (e.g. Aðalgeirsdóttir *et al* 2009) forced by ECHAM5 (A1B scenario) at the boundaries, (2) a ∼25 km resolution run of MAR (e.g. Fettweis 2007) (identical forcing as HIRHAM5), and (3) an ∼11 km resolution RACMO2 run (e.g. Angelen *et al* 2012), forced by HadGEM2 under the RCP4.5 scenario. All three model runs cover the whole of Greenland and are available for the years 1980–2098 at a temporal resolution of one day. Data from all DMI weather stations on Greenland are available for validation of the RCM data and for the correction of biases therein. The data (Boas and Wang 2011) cover the time period 1958–2010 and include 81, almost exclusively coastal, stations. However, numerous stations have been operating only for a limited period in the past.

While Mittivakkat glacier in south eastern Greenland is the only glacier with continued longer-term mass balances (1995–now) (cf Knudsen and Hasholt 2008) a large number of short-term mass balance observations exist (cf figure 1) and were obtained from publications (e.g. Hammer 2001, Ahlstrøm *et al* 2007), technical reports (e.g. Clement 1982), or gathered from the archives at the Geological Survey of Denmark and Greenland (GEUS), Copenhagen. Finally, measurements of ice thickness are available for a number of larger ice caps and valley glaciers on Greenland from the IceBridge project carried out by NASA (e.g. Gogineni *et al* 2001) and from other campaigns (e.g. Johnsen *et al* 1992, Hammer 2001, Citterio and Mottram 2008) (cf figure 1).

3. Mass balance modeling

Mass balance distribution for all glaciers of the six selected regions (section 2) is computed at a spatial resolution of

250 m. The applied glacier mass balance model is a simplified version of more sophisticated energy balance approaches. Here we briefly summarize the model as a detailed description is given by Machguth *et al* (2009).

The model runs at daily steps, and the cumulative mass balance b_c on day $t + 1$ is calculated for every time step and over each grid cell of the DEM according to Oerlemans (2001):

$$b_c(t + 1) = b_c(t) + \begin{cases} \Delta t \cdot (-Q_m)/l_m + P_{solid} & \text{if } Q_m > 0 \\ P_{solid} & \text{if } Q_m \leq 0 \end{cases}$$ (1)

where t is the discrete time variable, Δt is the time step (one day), l_m is the latent heat of fusion of ice (334 kJ kg^{-1}) and P_{solid} is solid precipitation in meter water equivalent (m w.e.). The energy available for melt (Q_m) is calculated as follows:

$$Q_m = (1 - \alpha)S_{in} + C_0 + C_1 T$$ (2)

where α is the albedo of the surface, T is the air temperature (in °C at 2 m above ground and outside the glacier boundary layer), and $C_0 + C_1 T$ is the sum of the long-wave radiation balance and the turbulent exchange linearized around the melting point (Oerlemans 2001). Global radiation (S_{in}) is calculated from potential clear sky global radiation ($S_{in,clr}$) and fractional cloud cover (n). Both the direct and diffuse part of $S_{in,clr}$ are computed in a preprocessing routine according to Corripio (2003); Iqbal (1983), considering all effects of surface topography including shading and assuming standard atmospheric transmission coefficients for clear sky conditions. During the mass balance model run, S_{in} of every individual time step is computed from preprocessed $S_{in,clr}$ and attenuation of clouds (τ_{cl}). The latter is derived from RCM fractional cloud cover at the actual time step according to an empirical relationship derived from observations on the Greenland ice sheet (GrIS) (Konzelmann *et al* 1994):

$$\tau_{cl} = 1.0 - bn^2 - \exp(-cz)$$ (3)

with $b = 0.78$ and $c = 0.00085$ being constants and z the surface elevation above sea-level.

The source of accumulation is precipitation (P) and a threshold temperature (T_{snow}) of 1.5 °C in combination with a transition range of 0.5 °C (i.e. linear increase of the rain fraction from 0% at 1 °C to 100% at 2 °C) is used to distinguish P_{solid} from rain. Redistribution of snow by wind or avalanches is not considered in the model. Refreezing is calculated according to Pfeffer *et al* (1991), expressing the amount of melt water (M) that can be retained as a ratio of annual accumulation (C):

$$\frac{M}{C} \geq \left[\frac{c}{l_m}T_f + \frac{\rho_{pc} + \rho_c}{\rho_c}\right]\left[1 + \frac{\rho_{pc} + \rho_c}{\rho_c}\right]^{-1}. \quad (4)$$

Thereby c refers to the heat capacity (1950 J K^{-1} kg^{-1}) of ice and ρ_{pc} is the pore close-off density (830 kg m^{-3}). The initial firn temperature (T_f) at the onset of the melt season (in positive degrees Celsius below freezing, (cf Pfeffer *et al* 1991)) is here calculated as the mean annual air temperature of the preceding three years. The initial firn density (ρ_c) is set equal to snow density and is derived from an empirical relationship based on observations from the GrIS (Reeh *et al* 2005):

$$\rho_c = 0.625 + 18.7T_f + 0.293T_f^2. \quad (5)$$

Glaciers are regarded as debris-free which is a reasonable assumption for the bulk of Greenland's GICs (cf Rastner *et al* 2012). Depending on the surface characteristics (snow, firn or ice) three different constant values for the surface albedo are used in the model: $\alpha_s = 0.75$, $\alpha_f = 0.55$ or $\alpha_i = 0.40$ (α_i calibrated to 0.35 for the regions 'South' and 'Mittivakkat', cf table 1). Accumulated snow is assigned α_f when its age exceeds 1 year and after 2 years its albedo is lowered to α_i. This parameterization aims at approximating the albedo lowering related to the snow aging and is not meant to simulate the actual conversion from snow to ice that take much longer on most of Greenland's glacier surfaces (e.g. Reeh *et al* 2005).

4. Coupling of mass balance model to RCM data

The mass balance model is forced from daily gridded RCM output. Rugged high mountain topography is not represented by the coarse spatial resolution of RCMs which is a main reason for biases or shifted pattern in meteorological variables (e.g. Franco *et al* 2012). The biases are addressed through (1) downscaling, (2) bias correction and (3) mass balance model calibration (cf Salzmann *et al* 2012, Machguth *et al* 2012). The three stages are described in the following sub-sections and their position in the modeling process is shown in figure 2.

4.1. Downscaling of the RCM data and bias correction

The simple downscaling procedure includes two steps: (1) The RCM grids (n, T and P) are interpolated to the resolution of the DEM (here 250 m) by means of inverse distance weighting (IDW) followed by (2) the application of sub-grid parameterizations (cf Machguth *et al* 2009). Prior to the interpolation of T the strong dependence on altitude is
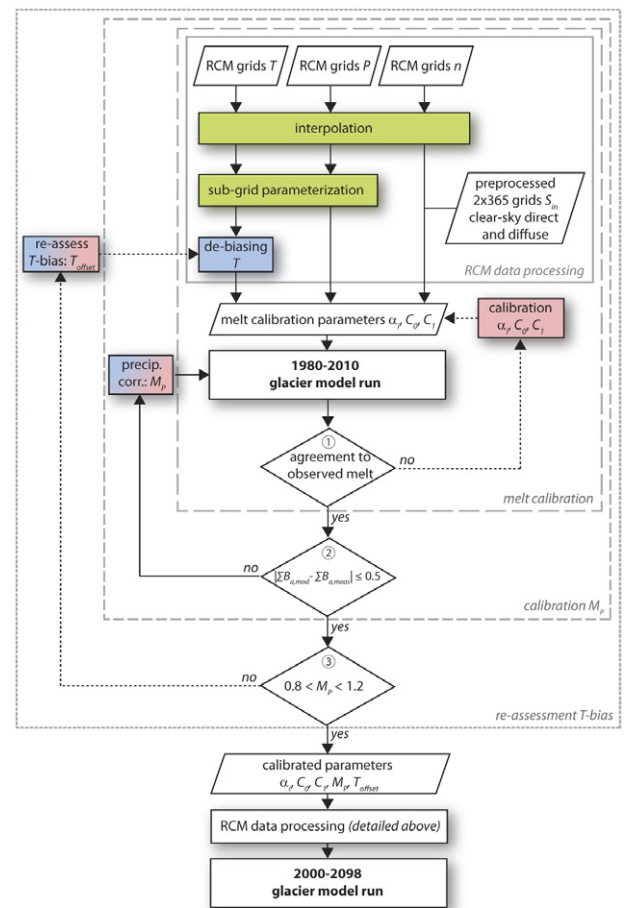

Figure 2. Flowchart of the modeling process. Steps related to the simple downscaling-approach are highlighted in light-green, de-biasing in light-blue and mass balance model calibration in light-red. Arrows with dotted lines denote manual steps. Note that for each region the conditions 1–3 are first tested for $\sum B_{a,\text{meas}} = \sum B_a$ *intermediate*. Calibrated values α_i, C_0 and C_1 and T_{offset} are then used in the calibrations to $\sum B_{a,\text{meas}} = \sum B_a$ *maximum* and $\sum B_a$ *minimum* where the conditional steps (1) and (3) are omitted.

removed by reducing T to a standard altitude $z_{\text{ref}} = 0$ m a.s.l. by means of altitudinal gradients γ_{Ti} where i denotes the number of the month (1–12). The atmospheric lapse rates γ_{Ti} were defined according to the empirically derived findings from Fausto *et al* (2009). We use the values derived by Fausto *et al* (2009) including the land stations. Fausto *et al* (2009) published only annual-mean and July γ_T and thus we reconstruct the lapse rates for the remaining months using linear interpolation.

In step (2) simple parameter specific (T, P, S_{in}) sub-grid parameterizations are applied to account for the major components of the small-scale influences of the rugged topography. Sub-grid scale variability of T is addressed by adjusting T from z_{ref} to the elevation of the DEM using the lapse rates γ_{Ti}. The same method is applied for P but the difficulty is to define a vertical gradient in precipitation (γ_P) as reliable observations of P in Greenland's mountain areas do not exist. As a proxy for γ_P we use observed winter mass balance distributions from the only two longer-term

mass balance series: The 10 year series from Amitsuloq ice cap in the south-west reveals a weak negative trend with altitude (cf Ahlstrøm *et al* 2007) while on Mittivakkat an increase in accumulation with elevation is observed (Knudsen and Hasholt 2008). The two series cannot be regarded representative for the whole of Greenland, but due to a lack of other data an intermediate value of 0.3 m precipitation increase per 100 m elevation increase was applied for all regions. It should be noted that γ_{Ti} and γ_P address only variability on the sub-grid scale and their influence decreases when the topography at the resolution of the mass balance model approaches the topography at the RCM resolution. Hence their influence is at maximum in rugged alpine topography and limited on larger ice caps.

The preprocessed grids of clear sky global radiation (section 3) account for the topographic sub-grid scale variability (i.e. exposition, slope and shading) while the temporally and spatially variable influence of cloudiness is derived directly from the interpolated fields of n (cf Machguth *et al* 2009). Cloudiness is directly interpolated to the resolution of the mass balance model by means of IDW because daily mean n is distributed rather smoothly in space.

Downscaled RCM fields require additional bias correction in T, S_{in} and P for accurate mass balance calculations (Machguth *et al* 2012). On Greenland, however, bias correction is hampered by the limited number of meteorological parameters being measured (only few weather stations do record S_{in} or n) but also by the fact that most weather stations are located directly at the coast and are not representative for higher elevations (e.g. due to frequent inversions, Hansen *et al* (2008)). In addition, comparing a coastal station with coarse resolution (11–25 km) RCM grid cells that might be of surface type 'ocean', bears the risk to establish unreasonable bias corrections. Hence a direct bias correction is performed (i) only for T and (ii) only for selected regions where suitable weather stations (located away from the open ocean) are available. Where these conditions are fulfilled (table 1) the mean deviation between observed and modeled T (1980–2010) for every day of the year was calculated. At every time step during the model run, T was then corrected by adding the offset to the downscaled temperature field. Note that this kind of bias correction does not change the future trends in T as prescribed by the RCM data.

4.2. Mass balance model calibration

Figure 2 visualizes the process of mass balance model calibration in the context of the full modeling chain. Calibration of the mass balance model is challenging because the driving RCMs are forced from GCM data, and thus modeled mass balance must be compared to observations representing climatological means. Hence model output (driven from downscaled and de-biased RCM data) for the time period 1980–2010 was compared to our 'best guess' in mean summer mass balance and total cumulative mass balance $\sum B_a$. We emphasize the term 'best guess' because in no case a complete 30 years time series is available: Mittivakkat (Knudsen and Hasholt 2008) is the longest series

(15 years in the time frame 1995–2010) and Amitsuloq (1981–1990) (Ahlstrøm *et al* 2007) the second longest.

Modeled summer-melt is adjusted to the measurements in a first calibration step ('melt calibration' in figure 2). However available summer mass balance observations do in most regions only cover one to three years which is too short for an automated and systematic adjustment of the model parameters. Thus calibration is restricted to a manual qualitative comparison and adjustment of model parameters C_0, C_1 and α_i (cf table 1).

After RCM downscaling, correction of T-bias and the aforementioned summer mass balance calibration, there is still considerable inaccuracy in modeled glacier mass balances. A main reason is the generally large differences of RCM precipitation pattern and the largely unknown real-world precipitation distribution (Machguth *et al* 2012). In addition, the RCMs are driven by ECHAM5 and HadGEM2 that fail to simulate the current climate over Greenland (Fettweis *et al* 2013). Such biases in the forcing GCMs impact the RCM results and affects our mass balance reconstruction. This explains why corrections are needed here. The comparison with the observations would be better if the RCMs were to be driven by reanalyses but no future projection is available in this case.

Hence it is justified to use P as an ultimate mean of model calibration ('calibration M_P' in figure 2). It was assumed that the modeled $\sum B_a$ 1980–2010 of each glacier must be identical to our best guess of observed $\sum B_a$ and P was tuned to achieve agreement. Our best guess of $\sum B_a$ was derived as follows: For the decade 1980–1990 we assumed that Greenland GICs were in a balanced state as it was roughly the case for the GrIS (Ohmura *et al* 1999) and Mittivakkat glacier (Knudsen and Hasholt 1999). For the decade 2000–2010 we assumed that the mass balance is well represented by the region specific mean ICESat derived mass balance for the time period 2003–2008 (Bolch *et al* 2013). Comparably little is known for 1990–2000 and we assumed that the mass balance has linearly decreased from the 80s to the value of the decade 2000–2010. The sum of the three decadal values is the region specific $\sum B_a$ which is assumed to be valid uniformly for all glaciers of a region. The latter assumption is a strong simplification but there is no data available to assess the variability within a region. The precipitation adjustment is performed individually for each modeled glacier to achieve $\sum B_a$ for 1980–2010. Only the cumulative mass balance is forced to be $\sum B_a$, variability of annual mass balance is not affected. Precipitation is varied iteratively by adjusting a temporally constant precipitation multiplication factor (M_P) until for each glacier a cumulative mass balance of $\sum B_a$ with a tolerance of ± 0.5 m w.e. results.

The calibration involves considerable uncertainties because in part, the GCMs that force the RCMs are not able to simulate the current mean climate and variability over Greenland. To assess their impact, model calibrations to three different values of $\sum B_a$ (*minimum, maximum and intermediate*, table 1) are performed. The three values are calculated for each selected region based on estimated uncertainty in the mass balance assumption for 1980–2010.

We assumed that each of the mass balance assumptions for the three decades has an (arbitrarily chosen) uncertainty of 25% of the total mass loss 1980–2010. Total uncertainty was calculated according to the laws of error propagation, assuming that the three decadal uncertainties are independent. The calibration to the three values of $\sum B_a$ was performed for all three RCM forcings and subsequently applied for the respective future scenario runs, resulting in: 3 RCM forcings $\times 3$ calibrations $= 9$ future scenarios for each region. All applied values of $\sum B_a$ for the selected regions are shown in table 1.

Any value of M_P below or above 1 will result in amplification or damping of the future trends in precipitation. To avoid strong modifications of the trend given by the GCM/RCM, calibrations to $\sum B_a$ *intermediate* were rejected when the regional mean M_P exceeds a (arbitrarily chosen) range of 0.8–1.2. Calibration was then repeated introducing a temperature offset (T_{offset}) applied uniformly to the entire region until M_P was within the limits ('re-assessment T-bias' in figure 2). We believe that such an additional bias correction for T is justified because (i) the aforementioned impact of M_P on future trends needs to be minimized and (ii), air temperature is subject to considerable uncertainties given the limited possibilities to determine bias in T (see section 4.1). Chosen T_{offset} are listed in table 1.

5. Glacier retreat modeling

5.1. Glacier bed topography calculation

Glacier bed topography is derived from modeled ice thickness. The chosen approach is based on the perfect plasticity assumption (cf Paterson 1994) and is described in full detail in Linsbauer *et al* (2012). Ice thickness is estimated at points along major central branch lines using an estimated basal shear stress (τ) of 125 000 Pa. The ice thickness (h) at every individual point is derived from the zonal surface slope α (surface slope around each point averaged over a 50 m elevation range along the branch lines) according to

$$h = \frac{\tau}{f \rho_i g \sin \alpha} \tag{6}$$

where f = shape factor (0.8), ρ_i = ice density (900 kg m^{-3}) and g = acceleration due to gravity (9.81 ms^{-2}). Hence, estimated ice thickness is a function of surface slope. From the estimated point values ice thickness is interpolated to the entire glacier surface and bed topography is calculated by subtracting the distributed ice thickness from the surface DEM (Linsbauer *et al* 2012).

The given approach provides a rough approximation of ice thickness. On the one hand calculated values on valley glaciers are in reasonable agreement with the few available observations (e.g. Citterio and Mottram 2008, Knudsen and Hasholt 1999). On the other hand modeled ice thickness is inaccurate on ice caps where the assumption of constant τ and f in connection with low quality DEM data in accumulation areas results in h of up to 2 km for ice caps with observed thickness of 400–600 m. Increasing f to 1, as appropriate

for the central parts of ice caps where there is no marginal strain (cf Paterson 1994), would reduce h by 20% but values are still outside of a realistic range. Finally an approach was chosen where modeled h is limited to observed maximum ice thickness (h_{max}) on the ice caps in the selected regions (table 1). After this correction modeled values are in the range of observations.

5.2. Parameterization of glacier retreat and volume change

Glacier retreat is simulated based on a Δh glacier retreat approach according to Huss *et al* (2010b). Glacier surface elevation change originating from ice dynamics and surface mass balance is parametrized by distributing volume gain or loss (resulting from the surface mass balance) over the entire glacier surface according to altitude dependent functions. These Δh functions (see next paragraph) are derived from previously observed changes in glacier thickness that incorporate both the influence of ice dynamics and surface mass balance. Glacierized grid cells become ice-free when their elevation falls below the altitude of the glacier bed. Glacier advance is not possible in the given approach. The Δh approach is mass-conserving with respect to the surface mass balance, i.e. mass loss or gain in the year m is converted into glacier thickness change and the DEM is updated at the onset of the year $m + 1$. Glacier surface mass balance calculation in the year $m + 1$ is performed on the updated topography and thus considers the feedback of surface elevation change on mass balance.

The applied Δh functions are derived from ICESat data for all GICs (Bolch *et al* 2013). For the four major regions of Greenland (cf Bolch *et al* 2013) an altitude-dependency of glacier thickness change and surface elevation can be derived (figure 3). The Δh functions are calculated from normalized elevation extent and changes in h are forced to be 0 at the highest point and 1 at the lowest. This does not fully agree with the observations in all regions, but is required to guarantee a proper functioning of the Δh approach. Huss *et al* (2010b) recommend using different Δh functions for different glacier size classes. We use the functions displayed in figure 3 uniformly for all glaciers of a region because the number of ICESat points in insufficient to derive glacier-type specific Δh functions.

6. Sensitivity analysis

A sensitivity analysis is performed in a similar manner as presented by Salzmann *et al* (2012). Thereby (i) the influence of an expected albedo decrease was investigated by gradually lowering α_i from 0.4 to 0.2 during the time period 2020–2040, (ii) the respective Δh function was modified towards a more pronounced mass loss at the tongue (active glacier retreat) and a more uniform mass loss over the entire area (down wasting). To limit computation time the sensitivity experiments were only performed for the regions Sukkertoppen and Zackenberg under HIRHAM5 forcing and $\sum B_a$ *intermediate* calibration.
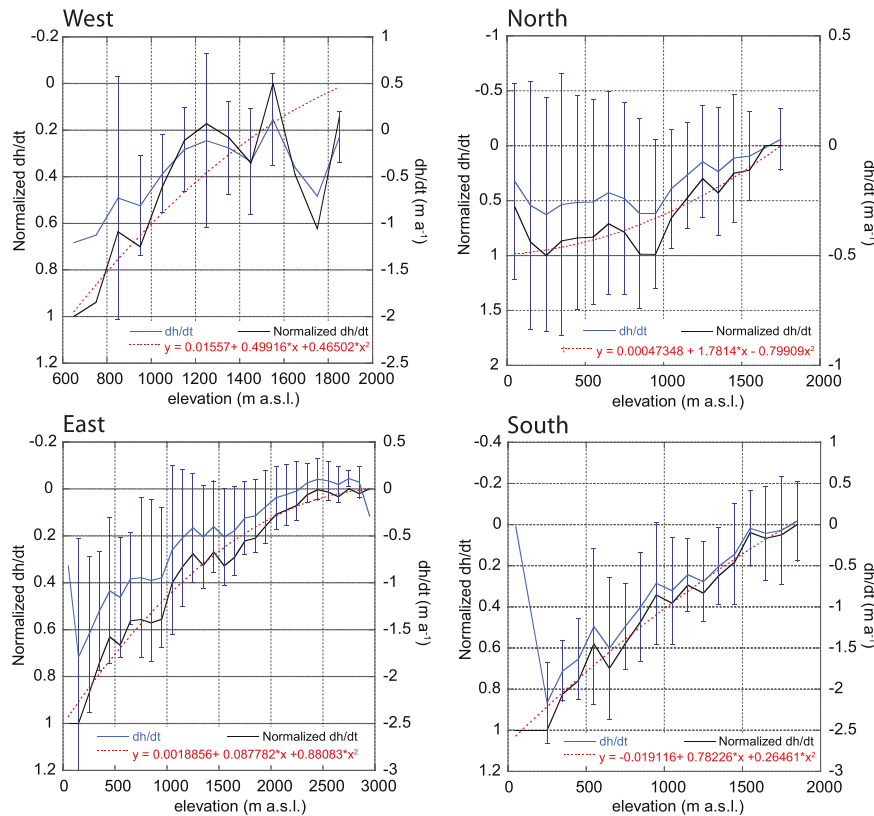
Figure 3. Observed dh/dt values (m a^{-1}), normalized dh/dt values and the derived Δh functions averaged over 100 m elevation intervals for the four main regions of Greenland (cf Rastner *et al* 2012, Bolch *et al* 2013, for the extent of the four regions). The error bars for dh/dt are given as 1σ of all dh/dt values in an elevation class. No standard deviation is calculated where less than five values are present in an elevation class.

7. Results

7.1. Modeled mass balance and glacier shrinkage

Our results indicate a decrease in ice volume for all six investigated regions. Thereby volume changes are smaller (-3% to -50%) from the central east to the very north and largest (-73% to -92%) in the south and south-east (figure 4). Absolute values of initial ice volume (V_{2000}) and area (A_{2000}) as well as final ice volume (V_{2098}) and area (A_{2098}) are given in table 2.

In general a realistic picture of modeled glacier retreat results (figures 5 and 6): The examples from the Sukkertoppen area show very pronounced retreat in the relatively moist near-coastal areas (figure 5(a)) and moderate changes of the Amitsuloq ice cap (figure 5(b)) which lies in the rain-shadow of larger ice caps and receives less precipitation. These results are in agreement with the expected larger climate sensitivity of more maritime glaciers (e.g. Oerlemans and Fortuin 1992). Mittivakkat glacier (figure 5(c)) has retreated by approx. 5 km by 2098, corresponding to a retreat rate of 50 m a^{-1}. The large valley glaciers in the Stauning Alper (figure 6) have retreated by 4–7 km, yielding an annual retreat rate of roughly 40–70 m.

The MAR forcing results in the strongest mass loss for all regions (figure 4) and differences to the HIRHAM5 forcing are significant although the two RCMs are forced by

the same GCM fields (ECHAM5 under the A1B emission scenario). The main reason for the stronger mass loss under MAR forcing is a more pronounced decrease in summer mass balance (B_s) (figure 7) in the north-eastern and northern regions. Trends in B_s in the southerly regions (Sukkertoppen, South and Mittivakkat) are more similar for all three forcings but MAR is still the most negative. More negative B_s must be related to a more pronounced warming. In a comparison study focused on the GrIS, Rae *et al* (2012) show that when downscaling the same GCM scenario (ECHAM5-A1B) MAR will have stronger future (2000–2099) warming trend than HIRHAM5. Thereby strongest deviations are observed in the north-eastern marginal regions of the ice sheet, close to the regions where this study finds the largest differences. However, the findings of Rae *et al* (2012) refer to the ice sheet while the mass balance model in the present study is mainly forced with RCM output from grid cells that are ice-free in the RCMs: when using MAR and HIRHAM5 78% of the area of the modeled GICs is located on RCM cells with surface type 'land'. RACMO2 cells can have fractional ice cover and the average ice cover fraction of the grid cells underlying the modeled GIC is 54%. HIRHAM5 and RACMO2 forcing result in similar glacier changes with mass loss being overall larger under RACMO2 forcing. All three forcing fields obtained with the RCM downscaling runs generate similar trends in winter mass balance (B_w) despite the different emission scenarios and GCM forcing fields:
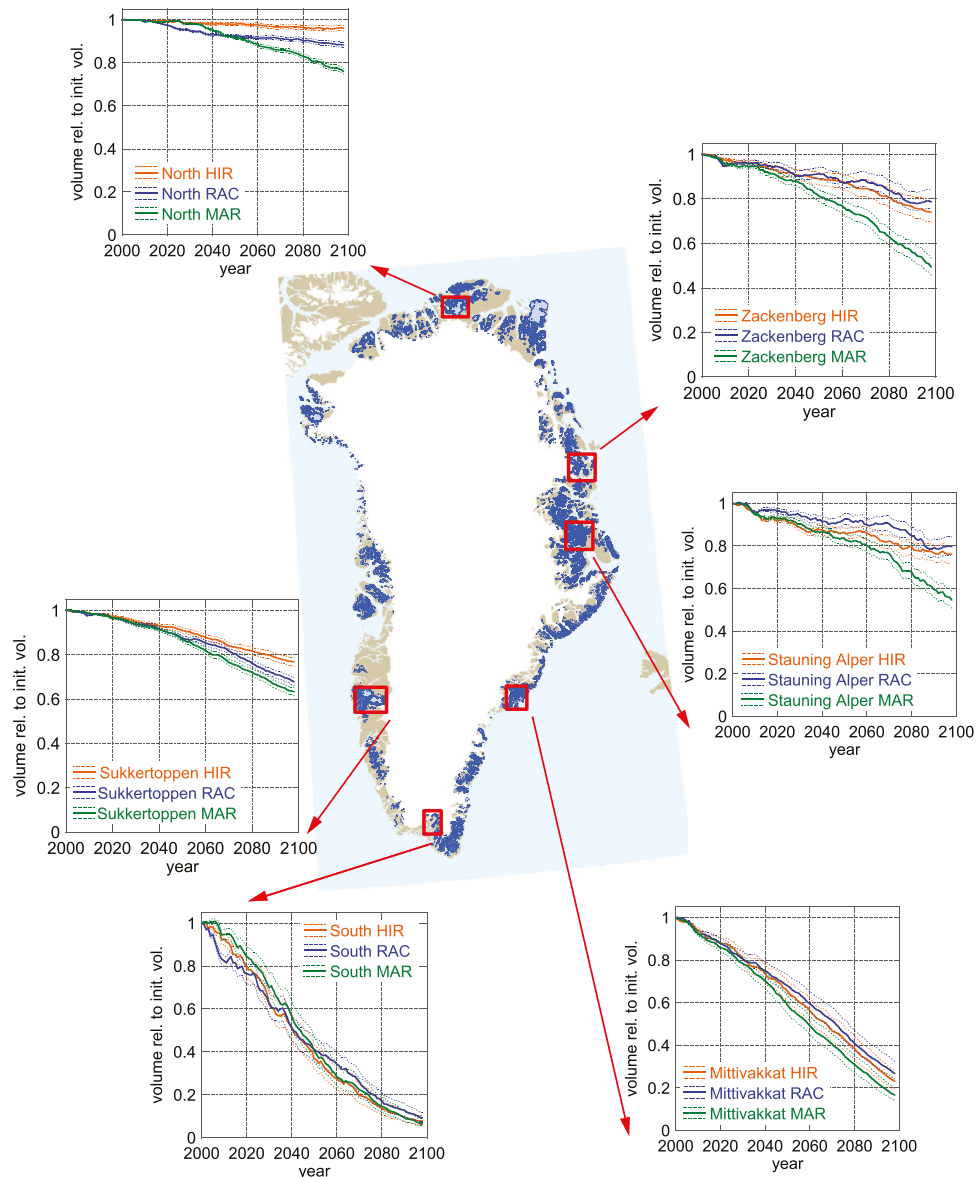
Figure 4. Volume change relative to the initial volume for all six selected regions (HIR = HIRHAM5 and RAC = RACMO2). The solid lines denote the mode calibration *intermediate* while the dashed lines represent the calibrations *minimum* and *maximum*.

B_w shows clearly increasing trends from the central east to the very north (Stauning, Zackenberg and North) and no trends for the more southerly regions. When forcing the model with the output from RACMO and HIRHAM5 the increase in B_w in the three northern regions almost counterbalances the decrease in B_s, under MAR the decrease in B_s dominates for all regions.

Figure 7 shows for the Mittivakkat region a systematically lower B_w under the MAR forcing. The reason is that MAR strongly underestimates precipitation in the area and that T was lowered by 1.5 K to avoid strong precipitation corrections that would impact on the future precipitation trend. However, the temperature lowering results in a smaller glacier mass turnover and thus likely a lower sensitivity to climate change. The issue could only be solved when precipitation is bias corrected without impacting on future trends. The Stauning Alper also show a lower value for B_w MAR. The reason is, however, different: B_s (MAR) over the

calibration period is less negative and hence model calibration results in lower precipitation.

The aforementioned issues in model calibration are one of the reasons to perform three different calibrations for each region and each RCM forcing. The volume changes under calibrations *minimum* and *maximum* are shown as deviations ($\pm$) in table 2. The sensitivity analysis reveals that gradually lowering α_i to 0.2 from 2020 to 2040 and holding the albedo constant afterwards increases the volume loss for Zackenberg by 13 km^3 or 24% compared to no albedo change. For the Sukkertoppen region the increase in volume loss reaches 78 km^3 or 29%. Modifying the Δh functions has a comparably small impact of approximately $\pm$2% for both regions.

7.2. Extrapolation to all Greenland GICs

We divided Greenland into five sectors to upscale modeled volume change from the modeled regions to the entire sectors
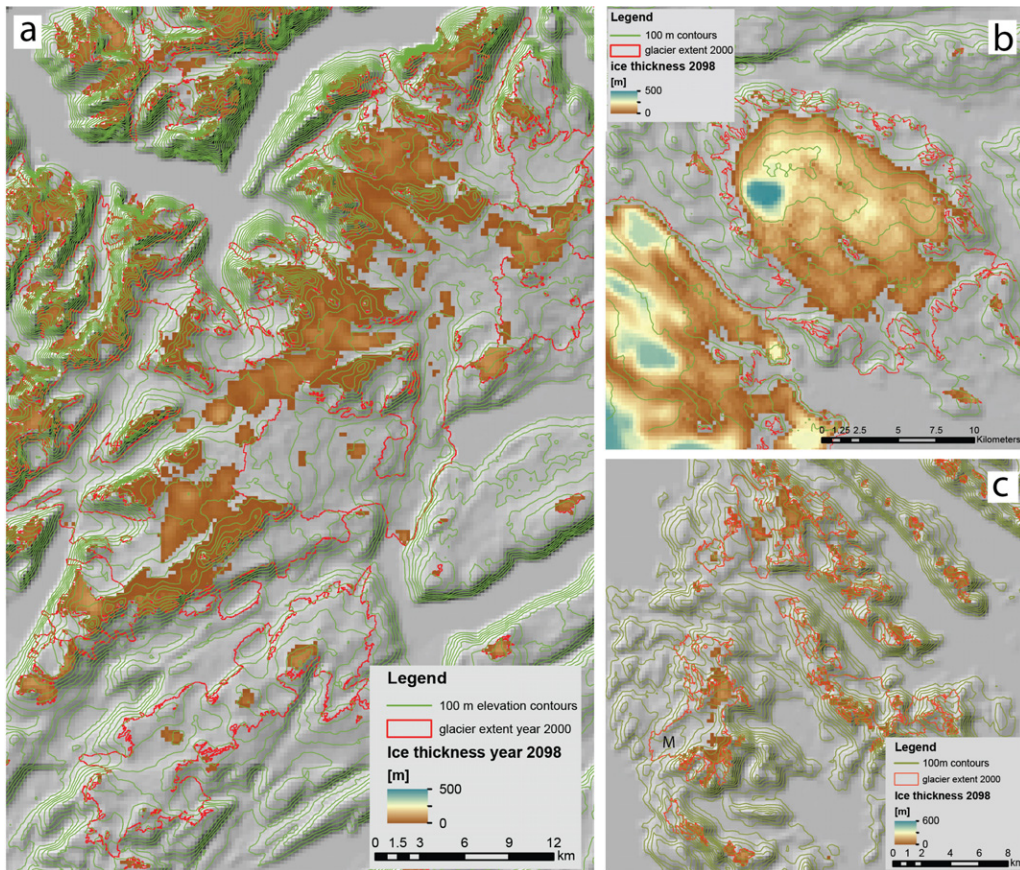
Figure 5. Examples of modeled glacier retreat (contour-lines represent surface topography in 2098): (a) Sukkertoppen region, modeled with RACMO2: South-west of the Sukkertoppen ice cap. The elongated ice cap in the south that has almost disappeared is the Tasersiaq ice cap which has a ten year record of mass balance observations. (b) Sukkertoppen region, modeled with RACMO2: The Amitsuloq ice caps to the north of Sukkertoppen. The ice cap has a ten year record of extensive mass balance observations. (c) A section of Mittivakkat region with Mittivakkat glacier ('*M*' on the map), modeled with HIRHAM5.

Table 2. Overview of modeled initial and final glacier volume and area in the six selected regions (A_{2000}, A_{2098} in km^2; V_{2000}, V_{2098} in km^3). The given values are based on the calibration to $\sum B_a$ *intermediate* while the deviations ($\pm$) are calculated from the calibrations *maximum* and *minimum*.

Region	Model	A_{2000}	A_{2098}	V_{2000}	V_{2098}
North	HIRHAM5	4446	4386 ± 25	777	745 ± 10
	RACMO2		4087 ± 48		685 ± 9
	MAR		3665 ± 57		590 ± 10
Zackenberg	HIRHAM5	1541	1210 ± 77	206	151 ± 10
	RACMO2		1333 ± 56		161 ± 9
	MAR		875 ± 61		101 ± 8
Stauning	HIRHAM5	3884	3402 ± 83	327	255 ± 14
	RACMO2		3490 ± 85		266 ± 15
	MAR		2744 ± 149		182 ± 13
Mittivakkat	HIRHAM5	2222	805 ± 142	311	72 ± 14
	RACMO2		874 ± 114		84 ± 13
	MAR		538 ± 108		52 ± 9
South	HIRHAM5	170	31 ± 6	7.8	0.6 ± 0.2
	RACMO2		28 ± 6		0.7 ± 0.2
	MAR		27 ± 6		0.7 ± 0.1
Sukkertoppen	HIRHAM5	5398	4325 ± 90	1180	910 ± 23
	RACMO2		4006 ± 90		804 ± 21
	MAR		3617 ± 100		751 ± 21

Table 3. Volume loss area scaling relationship calculated from the modeled volume loss of the six selected regions. For simplicity only the values based on the calibration to $\sum B_a$ *intermediate* are given.

Selected region	a			λ		
	HIRHAM5	RACMO2	MAR	HIRHAM5	RACMO2	MAR
North	0.004 5871	0.037 1580	0.029 589	1.0795	0.885 07	1.0645
Zackenberg	0.033 6320	0.027 6310	0.048 589	1.0113	1.008 00	1.1294
Stauning	0.006 1142	0.005 5372	0.018 061	1.2330	1.234 10	1.1843
Mittivakkat	0.033 3000	0.033 9930	0.034 105	1.2967	1.286 80	1.3084
Sukkertoppen	0.027 8680	0.025 1590	0.028 043	1.0928	1.191 20	1.1941
South	0.020 0270	0.020 8730	0.020 783	1.3689	1.347 90	1.3582

Table 4. The five sectors of Greenland and extrapolated volume loss 2000–2098. The given values are based on the calibration to $\sum B_a$ *intermediate* while the deviations ($\pm$) are calculated from the calibrations *maximum* and *minimum*.

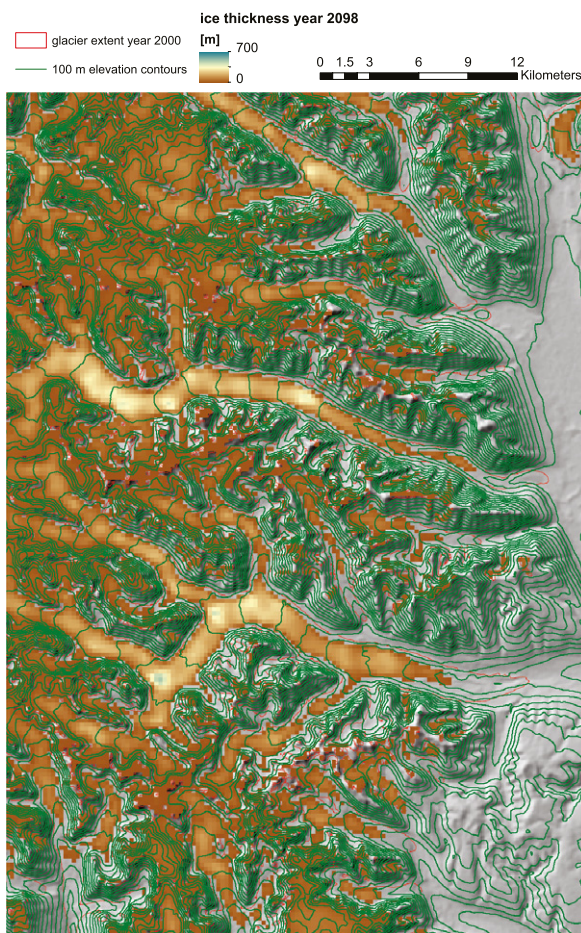| Sector	Selected region	A_{2000} (km^2)	ΔV (km^3)		
			HIRHAM5	RACMO2	MAR
North	North	39 327	-277 ± 98	-829 ± 77	-1548 ± 93
East-North	Zackenberg	5 789	-200 ± 46	-163 ± 36	-274 ± 9
East-Central	Stauning	21 618	-302 ± 72	-275 ± 67	-742 ± 64
East-South	Mittivakkat	10 220	-970 ± 44	-952 ± 42	-1042 ± 14
West	Sukkertoppen	12 765	-491 ± 41	-652 ± 33	-735 ± 37
Total		89 719	-2240 ± 143	-2871 ± 121	-4341 ± 120

Figure 6. Stauning Alper: modeled glacier retreat (using MAR) for a number of valley glaciers. The elevation contours represent surface topography in 2098.

(figure 1). The sectors were chosen in a way that all of the GICs are best represented by one of the modeled regions. Thereby only five regions are used and region South is omitted because the glaciers are too small to be representative for larger neighboring ice bodies. For each of the five selected regions all modeled individual glaciers are used to calculate a regression in the form of a power law $V_{2000} - V_{2098} = \Delta V = aA_{2000}^\lambda$, where a and λ are coefficients and A_{2000} is the surface area in the year 2000. Hence the regression explains the volume loss from 2000 to 2098 as a function of initial surface area; regression coefficients R^2 are by average 0.93 with a minimum of 0.87 and a maximum of 0.99. The regression deals with the volume loss, not with the total glacier volume and should consequently not be mistaken for regular volume–area scaling (e.g. Bahr *et al* 1997). Nevertheless table 3 shows that for regions with almost complete ice loss (e.g. South) λ approaches values typically used to estimate total glacier volume in volume–area scaling (1.3–1.4, cf Bahr *et al* 1997). For areas with low mass loss λ is close to 1 (e.g. Zackenberg). Using the regional power laws (table 3) and the individual areas of all glaciers of the corresponding sectors (according to the Greenland glacier inventory) the total ΔV of each sector was derived (table 4). Greenland's GIC are predicted to lose 2240 $\pm$ 143 km^3 of volume until 2098 (HIRHAM5 forcing), when forced by RACMO2 the volume loss is 2871 $\pm$ 121 km^3 and for MAR 4341 $\pm$ 120 km^3. Deviations ($\pm$) from the intermediate values are calculated according to the laws of error propagation assuming that deviations in the different sectors are independent (we avoid the term 'uncertainty' because only sensitivity studies were performed). Converting volume loss to mass loss assuming density ρ_i yields a loss of 2016 $\pm$ 129 Gt (HIRHAM5), 2584 $\pm$ 109 Gt (RACMO2) and 3907 $\pm$ 108 Gt (MAR), corresponding to sea-level equivalents of 5.8 $\pm$ 0.4, 7.4 $\pm$ 0.3 or 11.2 $\pm$ 0.3 mm, respectively.
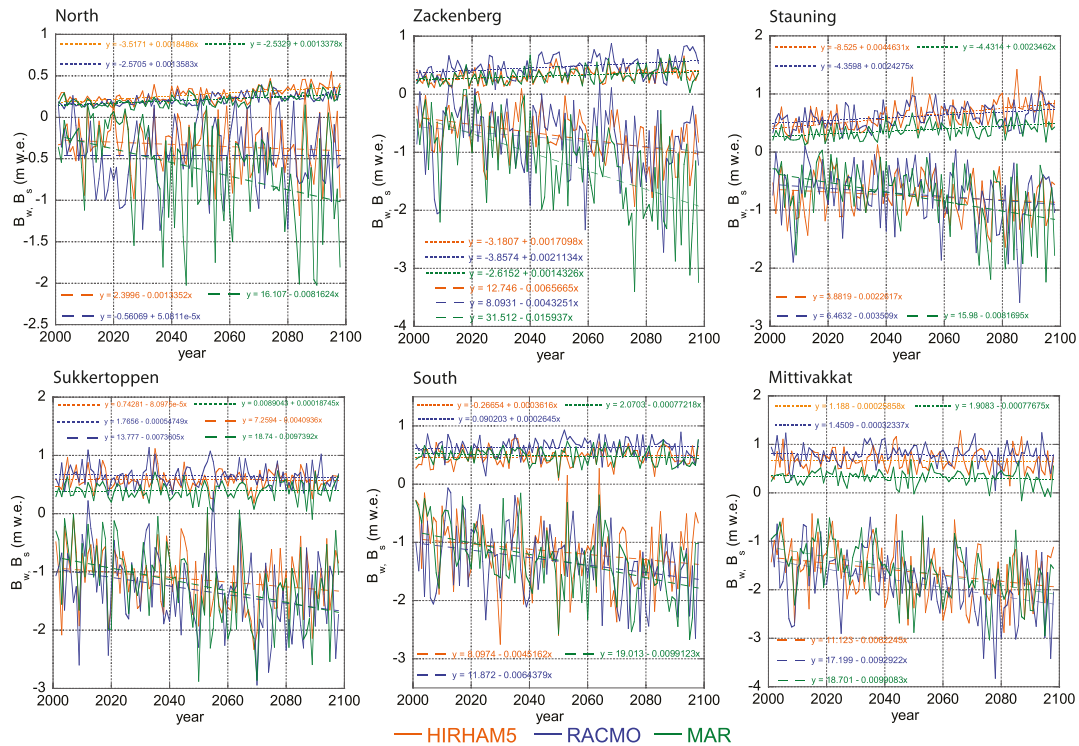
Figure 7. Mean annual summer (B_s) and winter (B_w) mass balance for the six selected regions using calibration *intermediate*.

8. Discussion and conclusions

In the present study sea-level rise contribution from all local glaciers and ice caps on Greenland is modeled and a range of projections is defined by (i) using three different RCM forcings, (ii) performing three different mass balance model calibrations under each RCM forcing, and (iii) performing a sensitivity analysis to explore the effect of a potential decrease in ice albedo and variations in the applied Δh functions.

The choice of the forcing field strongly impacts on modeled sea-level rise contribution. Interestingly the results from the two RCM that are forced with the same GCM output fields divert the most. A likely reason for these differences is the positive albedo feedback that enhances the warming and is considered in MAR but not in HIRHAM5. RACMO2 also takes into account the surface albedo feedback and this could partly explain the stronger mass loss under the RCP4.5 scenario (HadGEM2 RACMO2 forcing) compared to A1B (ECHAM5 HIRHAM5 forcing). The mass balance model calibration has for most regions a smaller impact. A statistical uncertainty range cannot be calculated based on three RCM forcings and hence we provide only modeled mass loss for the three forcings with their respective deviations resulting from the calibrations. The albedo sensitivity experiment indicates that lowering the ice albedo to 0.2 by 2040 increases mass loss by roughly 20–30%. A clear lowering trend in surface albedo is currently observed in the ablation area of the GrIS (Box *et al* 2012). However, future projections of albedo change are of a speculative nature and therefore we do not consider the impact of albedo lowering in the final numbers. Nevertheless, the sensitivity experiment indicates that the given final numbers of mass loss are lower boundary estimates.

The modeled annual sea-level rise contribution (0.059 ± 0.004 mm HIRHAM5, 0.076 ± 0.003 mm RACMO2 and 0.114 ± 0.003 mm yr^{-1} MAR) are in the range of the current contribution of 0.08 ± 0.03 mm yr^{-1} from 2003 to 2008 (Bolch *et al* 2013). Given the continued warming trend a higher contribution than observed today could be expected. The most likely reasons for the modeled rate of mass loss being similar to current observations are (i) the use of mid-range scenarios, (ii) the predicted increase in precipitation over large areas of GICs in the north-east and north, (iii) the fact that the fastest melting parts of the glaciers disappear first which results in an asymptotic behavior of the mass loss rate and (iv) the exclusion of all calving processes from the modeling chain. According to Bolch *et al* (2013) the rate of mass loss of calving glaciers is 10% higher than for non-calving glaciers. However, continued glacier retreat might eventually reduce the impact of calving for many regions and a substantial part of the ice lost due to calving is below sea-level and will thus not contribute to sea-level rise.

The sea-level rate computed by Radić and Hock (2011) (0.036 ± 0.02 mm yr^{-1}) is only about half (when forced by HIRHAM5 and RACMO output fields) or a third (when forced by MAR output) of our results. However, Radić and Hock (2011) underestimated the surface area of Greenland's GICs. When comparing mass loss per area-unit (here and in the following mass loss per area-unit is calculated based on the initial surface area used by the various studies) and considering also the uncertainties given by Radić and Hock (2011), the two studies are in reasonable agreement. Then again Marzeion *et al* (2012) have calculated a higher sea-level rise contribution from Greenland's GICs under the

RCP4.5 scenario (approx. 0.16 mm yr^{-1} until 2100). In the following we put these scenarios into the context of GrIS future scenarios: modeled future sea-level rise contribution (2000–2100) from the GrIS using a set of GCMs under the A1B scenario indicate 1.5–6.5 cm with a median of 4 cm (according to Fettweis *et al* 2008, considering only changes in surface mass balance) or 0–17 cm with a mean of 4.5 cm (according to Graversen *et al* 2010, considering also dynamic mass loss). Fettweis *et al* (2013) find a sea-level rise contribution from the GrIS surface mass balance of 4 ± 2 cm by 2100 (RCP4.5 scenario). In this context the modeled contributions from Greenland GICs are remarkably large: according to Rastner *et al* (2012) the GICs area corresponds to only 5.4% of the GrIS and if the GrIS' future mass loss per area-unit were the same as modeled in the present study for the GICs, the GrIS' future (2100) sea-level rise contribution would be roughly 11 cm (HIRHAM5, A1B), 21 cm (MAR, A1B) or 14 cm (RACMO2, RCP4.5). Comparing these numbers with the aforementioned projections for the GrIS (Fettweis *et al* 2008, Graversen *et al* 2010, Fettweis *et al* 2013) shows that our study and Radić and Hock (2011) indicate a higher (by approx. a factor of three to four) sensitivity to climate change for the GICs while the results of Marzeion *et al* (2012) suggest mass loss per area-unit being roughly seven to eight times larger on the GICs than on the GrIS. According to Bolch *et al* (2013) the observed (2003–2008) mass loss per area-unit is about two to three times larger on the GICs than on the GrIS.

Glaciers with low accumulation at the ELA are less sensitive to a given change in climate than more maritime glaciers (e.g. Oerlemans and Reichert 2000). Our results are in good agreement with this general law of glacier sensitivity, but the characteristics of glacier climate sensitivity are not the sole reason for the modeled smaller changes in the dry and cold north-east and the north. On the one hand mass loss in these areas would be larger if precipitation remained constant. On the other hand precipitation increase in a warming climate also leads to a change in glacier characteristics. For instance the glaciers in the Stauning Alper at the end of the 21st century show average values of winter and summer balances (RACMO2 and HIRHAM5 forcing) comparable to the glaciers in the Mittivakkat region at the beginning of the century. This change in glacier characteristics towards increased mass turnover and consequently larger climate sensitivity is a major challenge for future projections. Stating that glaciers in cold and dry climates will play a minor role among sea-level rise contributers due to their low climate sensitivity, neglects the impact of a change in climate on glacier's climate sensitivity.

It is a major strength of the chosen modeling approach to deliver comprehensible maps of glacier change and thereby including important feedback processes. Nevertheless, our sea-level rise projections for Greenland's GICs are based on several models and assumptions introducing various sources of uncertainty. By means of different calibrations and sensitivity experiments a number of them have been addressed. Further research is required to assess uncertainties related to model-design and thus we conclude by highlighting two major challenges for model improvement:

(1) 2 m air temperatures used for input to the mass balance model are influenced by the surface properties of the RCM grid cells (i.e. bare land, sea or ice). By adjusting the parameters C_0 and C_1 the mass balance model can be calibrated for use with 2 m air temperature from within or outside a glacier boundary layer (cf Citterio *et al* 2011). Inconsistencies, however, result where the calibration and the RCM surface type do not match. This is a minor issue with the coarse MAR or HIRHAM5 grids where roughly 80% of the modeled GICs are located on RCM cells of the type 'land', but it becomes important when using RACMO2 with its more detailed glacier mask. One solution might be the use of a spatially varying calibration. Another approach would be reducing the influence of the RCM's surface properties on surface air temperatures by reconstructing the latter from temperatures in the free atmosphere using methods similar to Jarosch *et al* (2012).

(2) Important issues arise from the modeling of the ice caps: firstly the inaccuracies in the simple approach to assess bed topography need further investigation and comparison to alternative approaches (e.g. Huss and Farinotti 2012). Secondly, the application of the Δh approach to ice caps bears the risk of underestimating elevation changes in the accumulation areas. Originally developed for valley glaciers (Huss *et al* 2010b), the approach assumes that the highest point of a glacier does not change elevation. Observed changes on ice caps, however, are more complex: some ice caps are thickening in their accumulation areas and thinning in the ablation zone (Rinne *et al* 2011) while others are only thinning (e.g. Bolch *et al* 2013). None of the existing coupled glacier mass balance and ice dynamics models are capable to fully address the complexity of volume changes of ice caps. Nevertheless benchmarking the Δh approach on selected ice caps against dynamic models would help to quantify possible underestimation in elevation change.

Acknowledgments

References

Aðalgeirsdóttir G, Stendel M, Christensen J H, Cappelen J, Vejen F, Kjær H A, Mottram R and Lucas-Picher P 2009 Assessment of the temperature, precipitation and snow in the RCM HIRHAM4 at 25 km resolution *Danish Climate Centre Report* 09-08 (Copenhagen: Danish Meteorological Institute)

Ahlstrøm A P, Bøggild C E, Olesen O B, Petersen D and Mohr J J 2007 Mass balance of the Amitsulôq ice cap, West Greenland *Glacier Mass Balance Changes and Meltwater*

Discharge (*IAHS Publication* vol 318) (Wallingford: IAHS Press) pp 107–15

Angelen J H V, Lenaerts J T M, Lhermitte S, Fettweis X, Munneke P K, van den Broeke M R, van Meijgaard E and Smeets C J P P 2012 Sensitivity of Greenland ice sheet surface mass balance to surface albedo parameterization: a study with a regional climate model *Cryosphere* **6** 1175–86

Bahr D B, Meier M F and Peckham S D 1997 The physical basis of glacier volume–area scaling *J. Geophys. Res.* **102** 20355–62

Boas L and Wang P R 2011 Weather and climate data from Greenland 1958–2010, observation data with description *Technical Report* 11–15 (Copenhagen: Danish Meteorological Institute)

Bolch T, Sandberg Sørensen L, Simonsen S B, Mölg N, Machguth H, Rastner P and Paul F 2013 Mass loss of Greenland's glaciers and ice caps 2003–2008 revealed from ICESat laser altimetry data *Geophys. Res. Lett.* at press (doi:10.1002/grl.50270)

Box J E, Fettweis X, Stroeve J C, Tedesco M, Hall D K and Steffen K 2012 Greenland ice sheet albedo feedback: thermodynamics and atmospheric drivers *Cryosphere* **6** 821–39

Citterio M, Fausto R S and Machguth H 2011 Glaciological hydropower feasibility in the Qasigiannguit area, West Greenland: technical report *Technical Report* (Copenhagen: Geological Survey of Denmark and Greenland)

Citterio M and Mottram R 2008 Glaciological investigations at Malmbjerg, Stauning Alper, East Greenland: field report and results of GPR surveys *Technical Report* (Copenhagen: Geological Survey of Denmark and Greenland)

Clement P 1982 Glaciologiske undersøgelser i Johan Dahl Land 1981 *Tech. Rep.* (Grønlands Geologiske Undersøgelse)

Corripio J 2003 Vectorial algebra algorithms for calculating terrain parameters from DEMs and solar radiation modelling in mountainous terrain *Int. J. Geogr. Inform. Sci.* **17** 1–23

Fausto R S, Ahlstrøm A P, van As D, Bøggild C E and Johnsen S J 2009 A new present-day temperature parameterization for Greenland *J. Glaciol.* **55** 95–105

Fettweis X 2007 Reconstruction of the 1979–2006 Greenland ice sheet surface mass balance using the regional climate model MAR *Cryosphere* **1** 21–40

Fettweis X, Franco B, Tedesco M, van Angelen J H, Lenaerts J T M, van den Broeke M R and Gallée H 2013 Estimating Greenland ice sheet surface mass balance contribution to future sea level rise using the regional atmospheric climate model MAR *Cryosphere* **7** 469–89

Fettweis X, Hanna E, Gallée H, Huybrechts P and Erpicum M 2008 Estimation of the Greenland ice sheet surface mass balance for the 20th and 21st centuries *Cryosphere* **2** 117–29

Franco B, Fettweis X, Lang C and Erpicum M 2012 Impact of spatial resolution on the modelling of the Greenland ice sheet surface mass balance between 1990 and 2010, using the regional climate model MAR *Cryosphere* **6** 695–711

Gardner A S, Moholdt G, Wouters B, Wolken G J, Burgess D O, Sharp M J, Cogley J G, Braun C and Labine C 2011 Sharply increased mass loss from glaciers and ice caps in the Canadian Arctic Archipelago *Nature* **473** 357–60

Gogineni S *et al* 2001 Coherent radar ice thickness measurements over the Greenland ice sheet *J. Geophys. Res.* **106** 33761–72

Graversen R G, Drijfhout S, Hazeleger W, van de Wal R, Bintanja R and Helsen M 2010 Greenland's contribution to global sea-level rise by the end of the 21st century *Clim. Dyn.* **37** 1427–42

Hammer C U (ed) 2001 *The Hans Tausen Ice Cap: Glaciology and Glacial Geology* (*Meddelelser om Grønland: Geoscience* vol 39) (Copenhagen: Danish Polar Center)

Hansen B U *et al* 2008 Present-day climate at Zackenberg *Adv. Ecol. Res.* **40** 111–49

Howat I, Negrete A, Scambos T and Haran T 2013 A high-resolution elevation model for the greenland ice sheet

from combined stereoscopic and photoclinometric data (http://bprc.osu.edu/GDG/gimpdem.php)

Huss M and Farinotti D 2012 Distributed ice thickness and volume of all glaciers around the globe *J. Geophys. Res.* **117** F04010

Huss M, Farinotti D, Bauder A and Funk M 2008 Modelling runoff from highly glacierized alpine drainage basins in a changing climate *Hydrol. Process.* **22** 3888

Huss M, Jouvet G, Farinotti D and Bauder A 2010b Future high-mountain hydrology: a new parameterization of glacier retreat *Hydrol. Earth Syst. Sci.* **14** 815–29

Huss M, Usselmann S, Farinotti D and Bauder A 2010a Glacier mass balance in the south-eastern Swiss Alps since 1900 and perspectives for the future *Erdkunde* **64** 119–40

Iqbal M 1983 *An Introduction to Solar Radiation* (Toronto: Academic)

Jarosch A H, Anslow F S and Clarke G K C 2012 High-resolution precipitation and temperature downscaling for glacier models *Clim. Dyn.* **38** 391–409

Jiskoot H, Curran C J, Tessler D L and Shenton L R 2009 Changes in Clemenceau icefield and Chaba group glaciers, Canada, related to hypsometry, tributary detachment, length-slope and area-aspect relations *Ann. Glaciol.* **50** 133–43

Johnsen S J, Clausen H B, Dansgaard W, Gundestrup N S, Hansson M, Jonsson P, Steffensen J P and Sveinbjörnsdottir A E 1992 *A 'Deep' Ice Core From East Greenland* (*Meddelelser om Grønland: Geoscience* vol 29) (Copenhagen: Danish Polar Center) pp 1–22

Knudsen N T and Hasholt B 1999 Radio-echo sounding at the Mittivakkat gletscher, southeast Greenland *Arct. Antarct. Alp. Res.* **31** 321–8

Knudsen N T and Hasholt B 2008 Mass balance observations at Mittivakkat glacier, Ammassalik island, southeast Greenland 1995–2006 *J. Geogr. Tidsskr.—Dan. J. Geogr.* **108** 111–20

Konzelmann T, de Wal R V, Greuell W, Bintanja R, Henneken E and Abe-Ouchi A 1994 Parameterization of global and longwave incoming radiation for the Greenland ice sheet *Glob. Planet. Change* **9** 143–64

Linsbauer A, Paul F and Haeberli W 2012 Modeling glacier thickness distribution and bed topography over entire mountain ranges with GlabTop: application of a fast and robust approach *J. Geophys. Res.* **117** F03007

Machguth H, Haeberli W and Paul F 2012 Mass balance parameters derived from a synthetic network of mass balance glaciers *J. Glaciol.* **58** 965–79

Machguth H, Paul F, Kotlarski S and Hölzle M 2009 Calculating distributed glacier mass balance for the Swiss Alps from RCM output: a methodical description and interpretation of the results *J. Geophys. Res.* **114** 106

Marzeion B, Jarosch A H and Hofer M 2012 Past and future sea-level change from the surface mass balance of glaciers *Cryosphere* **6** 1295–322

Nuth C, Moholdt G, Kohler J, Hagen J O and Kääb A 2010 Svalbard glacier elevation changes and contribution to sea level rise *J. Geophys. Res.* **115**

Oerlemans J 2001 *Glaciers and Climate Change* (Lisse: A A Balkema Publishers)

Oerlemans J and Fortuin J P F 1992 Sensitivity of glaciers and small ice caps to greenhouse warming *Science* **258** 115–7

Oerlemans J and Reichert B 2000 Relating glacier mass balance to meteorological data by using a seasonal sensitivity characteristic *J. Glaciol.* **46** 1–6

Ohmura A, Calanca P, Wild M and Anklin M 1999 Precipitation, accumulation and mass balance of the Greenland ice sheet *Z. Gletscherkd. Glazialgeol.* **35** 1–20

Paterson W S B 1994 *The Physics of Glaciers* (Amsterdam: Elsevier)

Pfeffer W, Meier M and Illangasekare T H 1991 Retention of Greenland runoff by refreezing: implications for projected future sea level change *J. Geophys. Res.* **96** 22117–24

Radić V and Hock R 2011 Regionally differentiated contribution of mountain glaciers and ice caps of future sea-level rise *Nature Geosci.* **4** 91–4

Rae J G L *et al* 2012 Greenland ice sheet surface mass balance: evaluating simulations and making projections with regional climate models *Cryosphere* **6** 1275–94

Raper S C B and Braithwaite R J 2006 Low sea level rise projections from mountain glaciers and icecaps under global warming *Nature* **439** 311–3

Rastner P, Bolch T, Mölg N, Machguth H, Le Bris R and Paul F 2012 The first complete inventory of the local glaciers and ice caps on Greenland *Cryosphere* **6** 1483–95

Reeh N, Fisher D A, Koerner R M and Clausen H B 2005 An empirical firn-densification model comprising ice lenses *Ann. Glaciol.* **42** 101–6

Rinne E J, Shepherd A, Palmer S, van den Broeke M R, Muir A, Ettema J and Wingham D 2011 On the recent elevation changes at the Flade Isblink ice cap, northern Greenland *J. Geophys. Res.* **116** F03024

Salzmann N, Machguth H and Linsbauer A 2012 The Swiss Alpine glacier's response to the 2 °C air temperature target *Environ. Res. Lett.* **7** 044001

Weidick A and Morris E 1998 Local glaciers surrounding the continental ice sheets *Into the Second Century of Worldwide Glacier Monitoring—Prospects and Strategies* ed W Haeberli, M Hoelzle and S Suter (Paris: UNESCO) pp 197–205

Zwinger T and Moore J C 2009 Diagnostic and prognostic simulations with a full Stokes model accounting for superimposed ice of Midtre Lovénbreen, Svalbard *Cryosphere* **3** 217–29